Received: 17 April 2023 | Revised: 22 July 2023 | Accepted: 23 July 2023

DOI: 10.1002/app.54504

RESEARCH ARTICLE

Applied Polymer SCIENCE WILEY

Thermal conductivity aging and mechanical properties of polyisocyanurate (PIR) foams produced with different contents of HFO

Patricia Torres-Regalado[1,2] | **Mercedes Santiago-Calvo**[2] | **Josep Gimeno**[3] | **Miguel Angel Rodríguez-Pérez**[2,4]

[1]R&D Department, CellMat Technologies S.L., Valladolid, Spain

[2]CellMat Laboratory, University of Valladolid, Valladolid, Spain

[3]Honeywell S.L., Barcelona, Spain

[4]BioEcoUVA Research Institute on Bioeconomy, University of Valladolid, Valladolid, Spain

Correspondence
Miguel Angel Rodríguez-Pérez, CellMat Laboratory, University of Valladolid, Valladolid, Spain.
Email: marrod@uva.es

Funding information
Spanish Ministry of Economy, Industry, and Competitiveness, Grant/Award Number: DIN2019-010840; Ministerio de Ciencia, Innovación y Universidades, Grant/Award Numbers: PDC2022-133391-I00, TED2021-130965B-I00, PID2021-127108OB-I00, RTI2018 – 098749-B-I00; Regional Government of Castilla y León; EU-FEDER, Grant/Award Number: VA202P20; European Union NextGenerationEU/PRTR, Grant/Award Number: C17. I1

Abstract

Polyisocyanurate (PIR) foam is a thermal insulating material widely used in many industries such as construction, refrigeration, piping/tubing among others. In this research the production, characterization and modeling of the thermal conductivity of PIR foams synthesized with a hydrofluorolefin (HFO 1233zd (E)) as physical foaming agent have been studied. The results have shown that increasing the amount of HFO reduces the density, but the cellular structure is not modified. The relative mechanical properties are the same for the concentrations of HFO considered. In addition, the aging of thermal conductivity as a function of time has been studied in detail. The experimental results have been deeply analyzed using a theoretical model to predict the thermal conductivity The results show that the thermal conductivity and the rate of aging at early stages are reduced for the higher concentrations of HFO. This result has been related to the lower temperature reached during the foaming reaction for higher contents of the physical blowing agent.

KEYWORDS

environmentally friendly, hydrofluorolefins, modeling, physical foaming agent, polyisocyanurate foams, thermal conductivity

1 | INTRODUCTION

Rigid foams based on polyurethane (PU) are a fundamental part of our lives, since they are used in many fields such as for instance construction, refrigeration, and piping/tubing industries. These foams with a closed cellular structure are one of the most popular thermal insulators mainly due to their high insulating capability and excellent mechanical properties. In the construction sector, rigid PU (RPU) foams are used to make insulating panels, and to spray in situ to insulate the ceilings and the walls of the buildings and also the ventilation and the heating systems. In the refrigeration industry, RPU foams are employed as insulating materials because they offer a

high energy efficiency, good mechanical properties, good adhesion to the outer shells of the appliances, and an easily filling of the complex cavities of refrigerators. In the piping/tubing sector, RPU foams are used for insulating pipes since they reduce very efficiently the heat transfer between the conveyed medium and the environment. Inside the group of RPU foams polyisocyanurate (PIR) foams are included. These materials are produced using raw materials and formulations similar to those of RPU foams, except that the isocyanate index is higher and the polyol used is based on polyester instead of polyether.[1,2] PIR foams are typically considered an improved solution in comparison with RPU, due to their lower thermal conductivity, improved flame retardancy and higher temperatures of use.[3,4]

Physical blowing agents have been used for many years to produce RPU and PIR foams with low aged thermal conductivity. Initially, chlorofluorocarbon (CFCs) and later hydrochlorofluorocarbons (HCFCs) were the selected blowing agents, but they have been progressively replaced in many countries by isomers of pentane because of the high global warning potential (GWP) and ozone depletion potential (ODP) of the CFCs and HCFCs. However, although isomers of pentane are a good solution these blowing agents have a non-negligible global warming potential and are highly flammable. This last property creates safety risk during the production and during the use of the foams. Consequently, a new generation of foaming agents known as hydrofluoroolefins (HFOs) has been developed. HFOs are unsaturated organic compounds that comprise hydrogen, fluorine, and carbon. HFOs are being developed as a "fourth generation" of refrigerants. HFO products have short atmospheric lifetimes and are categorized as having close to zero ODP (Ozone Depletion Potential) and low GWP (Global Warming Potential), providing an environmentally friendly alternative. In addition, most of these blowing agents have a low flammability and some of them are non- flammable,[5–7] which increase the safety during foam production and use. For all these reasons, some previous publications have been focused on the use of HFOs as blowing agents for RPU and PIR foams. In one of published papers,[4] the aging behavior of RPU and PIR foams was analyzed measuring the concentration of blowing agent in the foams as a function of time. Another research[6] quantified the impact of temperature dependence on thermal conductivity in exterior walls and flat roofs on common insulating materials such as fiberglass, stone wool, polyisocyanurate, and extruded polystyrene using a temperature-dependent thermal conductivity profile. The results obtained for the different insulating materials were used in hygrothermal simulations in both continental and humid temperate climates. In another study,[7] the effect of the use of hydrofluorocarbons in air conditioning systems and their contribution to climate change was studied.

The scientific studies carried so far are not very detailed and there are many aspects regarding the use of HFOs in PIR foams that are still unknown such as the effect of these blowing agents on the reaction kinetics, on the cellular structure, on the mechanical properties and on the aged thermal conductivity for 25 years of aging. In fact, the production-structure-property relationships have not been studied in detail for these thermal insulating materials. This is, in fact, the main objective of this publication and its main novelty. In order to understand the thermal conductivity of PIR foams produced using HFO, it has to be considered that thermal conductivity is determined by the following heat transfer mechanisms[8–11]: conduction through the solid phase (λ_s), conduction through the gas phase (λ_g), thermal radiation (λ_r) and convection within the cells (λ_c) that is negligible for foams with small cell sizes (less than 2 mm).[12] The thermal conductivity of PIR foams mainly depends on the type and amount of blowing agents contained in the closed cells, due to the high contribution of λ_g to the total thermal conductivity (above 60%).[13,14] Moreover, another important aspect to consider is the aging of the PIR foam since the thermal conductivity values increase with time because the blowing agents used to produce the foam diffuse out of the cells, being replaced by atmospheric air, with a high thermal conductivity, which diffuses into the cells of the foam.[15–17]

On the other hand, the aging of the mechanical properties of PIR foams is also important. In the field of the aging of the mechanical properties of polyurethane, several studies have been carried out,[18] but as far as we know, no studies have been published on the aging of the mechanical properties of PIR foams produced with HFOs as physical blowing agent. This a second novelty of this research.

Considering the above, the aim of the present work is to evaluate, for the first time, the effect of different contents of an HFO blowing agent, HFO-1233zd(E) trans-1-chloro-3,3,3-trifluoropropene, on the reaction kinetics, density, cellular structure, the long-term thermal conductivity and mechanical properties of PIR foams. A systematic and comprehensive study is here presented to understand the production-structure-property relationships for these materials.

2 | MATERIALS AND METHODS

2.1 | Materials

The formulation of the PIR foams is based on the following components. The polyol component was a mixture of a polyester polyol (IP-9005 from Dow, USA), a non-silicone organic surfactant (Vorasurf 504 from Dow, USA), a trimerization catalyst (DabcoTMR-20 from

TABLE 1 Environmental data of physical blowing agents.[7,19–21]

Blowing agent	ODP (Ozone depletion potential)	GWP (Global warning potential)
N-Pentane	0	20
Isopentane	0	11
Cyclopentane	0	10
Methylal	0	<3
Solstice LBA	∼0	1

Evonik), a Mannich polyol (Voranol470x from Dow, USA) and distilled water obtained by reverse osmosis of 10 mega ohms per centimeter at 25°C. The isocyanate component was a polymeric methylenediphenyl diisocyanate (PMDI from Dow, USA). In addition, Solstice® LBA (also commercially labeled as HFO-1233zd(E) kindly supplied from Honeywell and based on trans-1-cloro-3,3,3-trifluoropropene) was used as physical foaming agent.

This blowing agent, Solstice® LBA, is more environmentally friendly than the current alternatives typically employed in PIR manufacturing,[7,9–21] as collected in Table 1.

Some interesting properties of Solstice® LBA (Honeywell), unlike other blowing agents available are: non-flammable (ASTM E681), VOC-free according to the Environmental Protection Agency (EPA), liquid near room temperature (boiling point at 19°C), zero ODP and GWP of 1.[7] Table 2 shows the main physical properties of the physical blowing agent used in this research.

TABLE 2 Physical properties of solstice HFO 1233zd(E).[7]

Chemical name	Trans-1-chloro-3,3,3-trifluoropropene
Molecular formula	(E)CF_3—CH═CCLH
CAS number	102687-65-0
Molecular weight (g/mol)	130
Atmospheric life	26 days
GWP	1
ODP	0
Boiling point	19°C/66°F
Flash point	None
Vapor flame limits	None
UN number	UN 3163
US DOT hazard class	LIQUEFIED GAS, N.O.S.
TLV/TWA	800 ppm
U.S. EPA ground-level ozone VOC	Exent compound

2.2 | Preparation of foamed samples

Polyisocyanurate foams with different contents of HFO were produced: 33.3 pph (33.3 parts per 100 parts of polyol), 38.3, 43.3, and 48.3 pph. These PIR foams were prepared using a three-step method using an IKA Eurostar 60 for mixing. Polyol (100 parts), trimerization catalyst (5 pph), Mannich polyol (5 pph), surfactant (4.5 pph) and water (2 pph) were mechanically agitated for 2 min at 250 rpm to ensure the complete homogenization of the components. After the initial step, the HFO physical blowing agent in the correct proportion (33.3, 38.3, 43.3, and 48.3 pph) was added to the blend and stirred for 2 min. During this step part of the HFO is evaporated and consequently it is necessary to incorporate an additional amount to have the exact content in the formulation. Before incorporating the isocyanate, the mixture is reweighed and the necessary HFO is added. Finally, the isocyanate was incorporated to the polyol premix, and the whole system was mechanically stirred at 2000 rpm for 10 s and poured into an open mold of dimensions 25 cm × 25.5 cm × 20.5 cm to allow the foam growth. One day after production, the foam was cut into samples with appropriate dimensions to characterize the materials and to measure the density, cellular structure characteristics, thermal conductivity and mechanical properties. The samples were stored after cutting in the following conditions: temperature 23 ± 2°C and humidity 50% ± 2% according to the ISO 291 standard.

2.2.1 | Foaming temperature measurements

The exothermicity of the reactive foaming process was experimentally measured by measuring the temperatures reached during foaming. These experiments were carried out in a plastic cup with 11.5 cm of diameter and 14 cm of height. Four thermocouples type K were placed vertically from the base and in the center of the plastic cup at the following heights: 0.5 cm (thermocouple 1, T1), 2.0 cm (thermocouple 2, T2), 6.5 cm (thermocouple 3, T3) and 12.5 cm (thermocouple 4, T4).[22] The mixing of the components was carried as previously explained. Once all the components were mixed, they were introduced in the plastic cup to determine the temperature during foaming. The data collected by the four thermocouples during foaming process were registered in a computer. Then, for each experiment the curves given by each thermocouple were averaged to obtain an average foaming temperature vs time curve. From these curves, the maximum value of the temperature for each system was obtained. Three experiments were carried out for each sample to obtain the average value.

2.3 | Characterization techniques

2.3.1 | Density and open cell content

Foam density was measured as described by ASTM D1622/D1622M-14.[23,24] The density was determined in three different cylindrical samples with 30 mm of diameter and 25 mm of height for each material.

After measuring the density, the open-cell content (OC) was measured with a gas pycnometer (Accupyc II 1340 from Micromeritics) using the same cylindrical samples, according to ASTM D6226-10.[24] Nitrogen was used as the displacement medium. OC was calculated by using the following equation:

$$\mathrm{OC}(\%) = 100\left(\frac{V_{\text{sample}} - V_{\text{pycnometer}} - V_S}{V_{\text{sample}} \cdot p}\right), \quad (1)$$

where V_{sample} is the geometrical volume of the sample (calculated from the sample dimensions), $V_{\text{pycnometer}}$ is the volume of the specimen measured with the pycnometer, V_S is the volume occupied by the cells located in the surfaces of the specimen calculated using $\left(\frac{A\times t}{1.14}\right)$ where A is the geometric surface area and t is cell size and p is the sample porosity calculated using $\left(1-\frac{\rho_{\text{foam}}}{\rho\text{solid}}\right)$ where ρ_{foam} is the foam density and ρ_{solid} the solid matrix density. A value of 1160 kg/m^3 was used for ρ_{solid}.[25]

2.3.2 | Cellular structure characterization

Scanning electron microscopy

The morphology of the cellular structure of these foams was evaluated by using scanning electron microscopy (SEM) with a HITACHI FlexSEM 1000. A plane including the growing direction (Z direction) of the cured foams was examined after vacuum coating the sample's surface with a gold monolayer. An image analysis tool specially designed to make a quantitative analysis of SEM micrographs was used to determine the main characteristics of the cellular structure[26]: average cell size in 3D (ϕ), anisotropy ratio (AR) and the standard deviation of the cell size distribution (SD). From these data, the normalized standard deviation of cell size distribution (NSD) was calculated as the ratio between the average cell size (ϕ) and the standard deviation of the cell size distribution (SD). This parameter can be related to the homogeneity of the cell size distribution. More than 150 cells of different areas of each material were used for the analysis.

X-ray tomography

The materials were also characterized by a laboratory x-ray tomography[27] to obtain the mass fraction in the struts (f_s). The set-up consists of an x-ray microfocus source (Hamamatsu) with a maximum output power of 20 W (spot size: 5 μm, voltage: 20–100 kV, current: 0–200 μA). X-rays come out of the source window, forming a cone-beam of 39°, allowing to obtain up to 20 times magnification. The transmitted X-ray intensity is collected with a high sensitivity flat panel connected to a frame grabber (Dalsa-Coreco), which records the projection images. This highest resolution detector is composed of a matrix of 2240 × 2344 pixels, each with a size of 50 μm. Cylindrical samples of about 20 mm^3 in volume were examined. The tube voltage was set at 50 kV, the tube current at 170 μA, the detector exposure time was 1 s, and each projection is the result of averaging three consecutive images to reduce noise. A configuration with the highest possible magnification was used, obtaining an effective pixel size of 2.5 μm. The approach to determine fs from the topographies has been detailed elsewhere.[27,28]

From the f_s obtained by tomography, the foam density and the cell size obtained from SEM, the average thickness of the cell walls δ has been calculated with the following equation:

$$(1-f_s)\cdot\phi\cdot\frac{\rho_{\text{foam}}}{\rho_{\text{solid}}} = C\cdot\delta, \quad (2)$$

where f_s is mass fraction in structs, ϕ is average the cell size, $\frac{\rho_{\text{foam}}}{\rho_{\text{solid}}}$ is the relative density of the foam, where ρ_{foam} is the foam density and ρ_{solid} the solid matrix density. A value of 3.35 was used for the constant C, that depends of the cell shape.[29]

2.3.3 | Mechanical properties

Mechanical properties were measured for all the foamed materials according to the standard ISO 844:2014.[30] These experiments were performed in compression using an Instron Machine (model 5.500R6025). Stress–strain curves were obtained at room temperature at a strain rate of 10 mm/min. The maximum static strain was 75% for all the experiments and the compression direction was parallel to the cell growth direction (thickness direction) of the foam. The samples were four cubes per material with dimensions of 50 × 50 × 50 mm^3. The experiments were performed 1 day after the foams production at 23 ± 2°C and humidity 50% ± 2%. Young's modulus (E) and collapse stress (σ_C) were calculated from the stress–strain curves.

Moreover, the aging of mechanical properties was studied for the sample produced with 48.3 pph LBA according to the procedure described in UNE-EN ISO 2440:2019.[31]

The initial mechanical properties were measured 72 h after foam synthesis. After that, the foamed samples were introduced into an oven at 80°C to age the samples. Subsequently, the measurements of mechanical properties were carried out 22, 96, 168, and 240 h after the material production. The mechanical tests were performed as it has described in the previous paragraph, with the same dimensions of samples and same strain rate.

2.3.4 | Thermal conductivity

Thermal conductivity measurements of the foams were performed using a Holometrix Rapid K heat flowmeter. The accelerated aging of thermal conductivity was measured according to the procedure described in ISO11561:1999 standard.[32] The initial thermal conductivity was measured 24 h after foam synthesis using a foamed block of 150 × 120 × 20 mm^3 (non-sliced sample). After measuring this sample, it was cut into two slices with the following dimensions: 150 × 120 × 10 mm^3 (sliced samples). These samples are stored in a room at 23 ± 2°C and a humidity of 50% ± 2%. Subsequently, the thermal conductivity of the stack formed by the two sliced samples was measured as a function of time up to 90 days after production. The 90 days are equivalent to 25 years aged value as indicated in the standard. The thermal conductivity measurements were carried out at 20°C, with a temperature gradient (ΔT) of 10°C.

3 | RESULTS AND DISCUSSION

3.1 | Characterization of PIR foams with different contents HFO

The main characteristics of the produced foams are collected in Table 3. The density of the samples is as expected, it decreases when the blowing agent content is increased in the foam formulation. Sample with the lowest content of HFO (33.3 pph) has the highest density (40 kg/m^3), whereas the sample with the highest HFO content (48.3 pph) reached 32.6 kg/m^3. The porosities of the samples are in the range of 96.6% to 97.2%. In general, all foamed samples have a closed cell cellular structure because the open-cell content is very low and in all cases below 5%. Moreover, the main characteristics of the cellular structure are summarized in Table 3 and the SEM micrographs of the samples are observed in Figure 1. Although the foams with different HFO content have different density, these materials have very similar cellular structures, as it can be appreciated in Figure 1. In fact, all foams have similar average cell sizes (around 900 microns) and a homogeneous cellular structure (NSD values are very low for all the materials). There is not a clear trend for these two structural parameters as a function of the HFO content.

Anisotropy ratio is always higher than 1, which relates to a slightly cell orientation in the growing direction. Values are in the range 1.23 to 1.32 with a slight increase of this parameter for the materials produced with larger amounts of HFO. Finally, the fraction of material in the struts ranges between 0.62 and 0.71 and the average cell wall thickness ranges between 1.7 and 2.3 microns. There is not a clear trend for these two parameters as a function of the HFO content.

3.2 | Mechanical properties

Measurements of the mechanical properties in compression (Young's modulus and collapse stress) of the PIR foams were first carried out at room temperature and 1 day after the foam production. As expected,[33] the mechanical properties, both the Young's modulus and collapse stress (Figure 2a,b), are reduced for the foams with lower densities (higher HFO contents).

Young's modulus and collapse stress divided by the relative density allow comparing the mechanical properties of PIR foams with different densities. The relative Young's modulus and the relative collapse stress of the foams are collected in Figure 3. It can be observed that the mechanical properties are similar for all the materials within the experimental accuracy except for the foam with 43.3 pph HFO which presents lower relative Young's modulus and collapse stress. This material presents a worse

TABLE 3 Density, open cell content (OC), porosity (p), average cell size (ϕ), standard deviation (SD), normalized standard deviation (NSD), anisotropy ratio (AR), fraction of mass in the struts (f_s) and wall thickness (δ) for each foam under investigation.

Sample	Density (kg/m^3)	P (%)	OC (%)	Φ (μm)	SD (μm)	NSD	A_R	f_s	δ (μm)
33.3 pph HFO	40.05 ± 0.66	97.2	2.53 ± 1.11	873	111	0.13	1.23 ± 0.21	0.65	2.3
38.3 pph HFO	38.10 ± 0.54	97.1	4.42 ± 0.46	871	102	0.12	1.24 ± 0.18	0.68	1.7
43.3 pph HFO	33.35 ± 0.34	96.7	1.36 ± 0.65	942	126	0.13	1.32 ± 0.22	0.71	2.2
48.3 pph HFO	32.60 ± 0.34	96.6	1.12 ± 0.66	872	129	0.15	1.32 ± 0.19	0.62	2.3

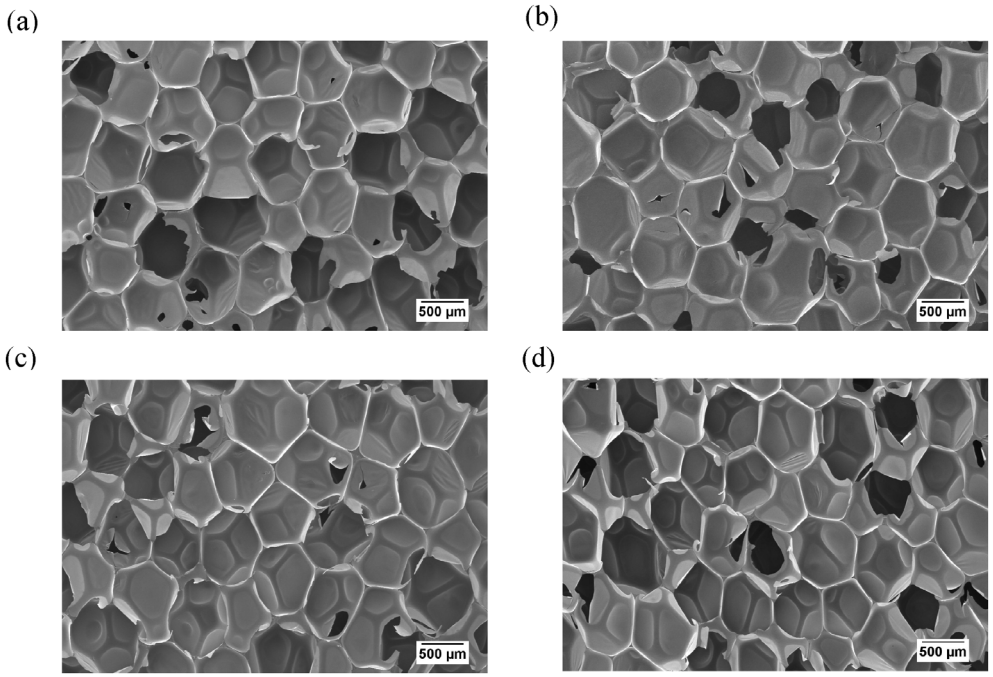

FIGURE 1 SEM micrographs of the foams under study showing the cell morphology of the samples with (a) 33.3 pph HFO, (b) 38.3 pph HFO, (c) 43.3 pph HFO and (d) 48.3 pph HFO.

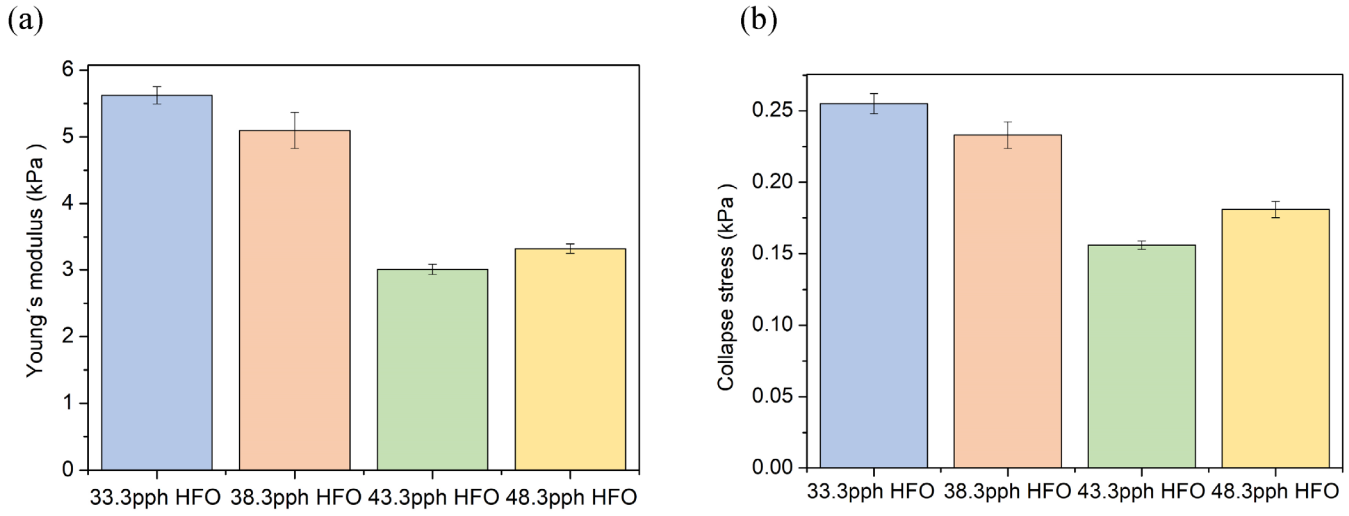

FIGURE 2 (a) Young's modulus and (b) Collapse stress for the PIR foams corresponding to compression tests. [Color figure can be viewed at wileyonlinelibrary.com]

mechanical behavior probably because it has a larger cell size and also a higher fraction of mass in the struts (Table 3). It is well know that these variations in the cellular structure results in foams with lower stiffness and strength.[34]

In addition, the sample with the highest content of HFO (48.3 pph) was selected to study the aging of the mechanical properties. The results obtained for density, Young's modulus, collapse stress, relative Young's modulus and relative collapse stress are shown in Figure 4. The results show that the density is slightly reduced during the aging process but the mechanical properties are hardly modified when the sample is subjected to an accelerating aging. Thus, the mechanical properties of this particular material are constant in the aging conditions used.

3.3 | Aging of the thermal conductivity

The thermal conductivity was measured over 90 days in order to study the accelerated aging of thermal conductivity (Figure 5), where the initial value was measured 1 day after the samples were manufactured and the

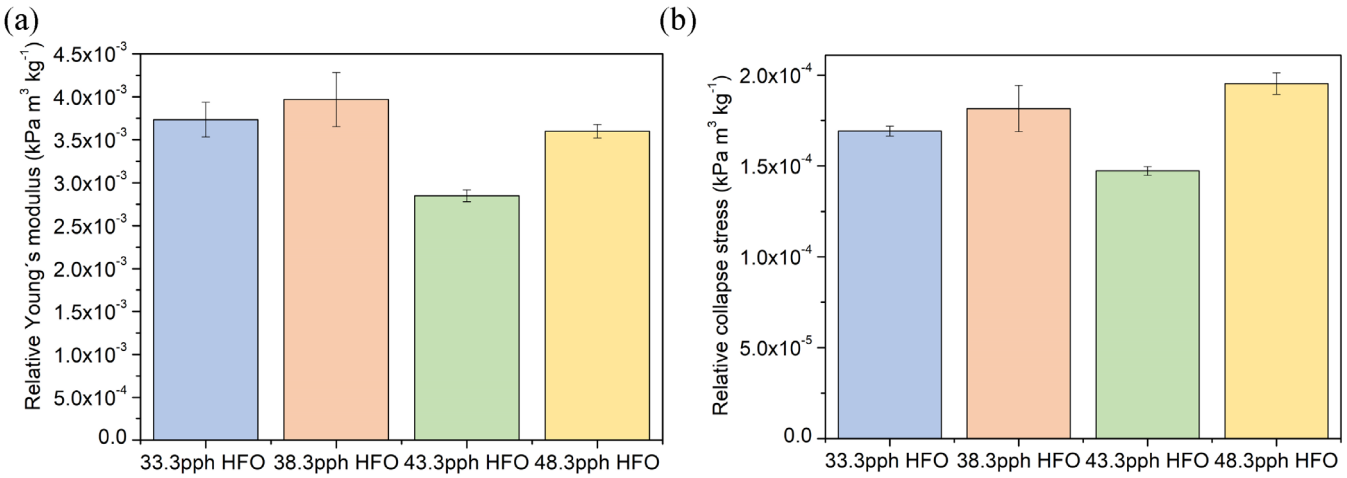

FIGURE 3 (a) Relative Young's modulus and (b) Relative collapse stress for the PIR foams produced with different contents of HFO. [Color figure can be viewed at wileyonlinelibrary.com]

measurements were continued until day 90, which corresponds to 25 years of aging according to the standard use for the tests.

The initial values of the thermal conductivity were very low, in the range of 20 to 22 mW/m K (Figure 5), but these values increase to reach values in the range 30 to 32 mW/m K after the aging process. During this aging there are two different periods of time. A rapid increase in the initial 15 days. In this period the values increase up to 27 to 29 mW/m K and then a slow increase from 15 to 90 days. Most of the initial increase of the conductivity is typically associated to the substitution of the CO_2 coming from the reaction of water and isocyanate by atmospheric air. The rest of the increase should be due to a slow diffusion of the HFO and its substitution by air. All foams behave in similar way but there are also differences among them. The results indicate that a larger amount of HFO is helpful to reduce the thermal conductivity at early stages and in the case of the material containing 48.3 parts of the HFO also after the aging. This is an important finding showing that an increase of the HFO content allows retaining a reduced thermal conductivity for a long period of time.

On the other hand, the parameter Delta Lambda ($\Delta\lambda$) was calculated along the 90 days This parameter measures the difference between the thermal conductivity at a given time (λ_t) and the initial thermal conductivity at (λ_0). Figure 6 shows $\Delta\lambda$ for PIR foams under study as a function of the aging time. It is observed that the aging of the thermal conductivity for the foam with 48.3 pph HFO is slower than for the rest of the contents, between the first day and the day 33. In addition, at early stages times it is clear that increasing the HFO content reduces the aging slope.

The rate of aging at low times for a PU system foamed with water and cyclopentane has been related in a previous work with the temperatures reached during the foaming process.[25] Due to this we also measured the temperature evolution during foaming for all the foams under study. Figure 7 shows the average foaming temperature versus time for these systems. It is observed that in general a lower content HFO is associated to higher temperatures during foaming. This makes sense because the evaporation of the blowing agent is an endothermic process and a higher amount of the blowing agent will reduce in a larger extend the temperature. Figure 8 shows that there is a clear relation between the maximum temperature reached during foaming and the slope of the thermal conductivity aging curve up to day 6 (day 6 was chosen as a representative day of early stages of aging. The general behavior is the same for other days in this period), indicating that also for this system the temperature reached during the reaction is modifying the aging curve in the initial stages. This is probably due to the different pressures developed inside the cells when the foaming temperature follows a different path.

These samples that achieve lower foaming temperatures (such as 48.3 pph HFO foam) exhibit lower thermal conductivity slopes (Figure 8).

3.4 | Modeling of thermal conductivity

Thermal conductivity modeling is proposed to further analyze the thermal conductivity aging of the samples under study. The thermal conductivity of a PIR foam (λ^t), containing solid and gas phases is well represented by the sum of four mechanisms: conduction along the cell walls and the struts of the solid polymer (λ^s), conduction through the gas phase (λ^g), thermal radiation (λ^r) and convection within the cells (λ^c). The addition

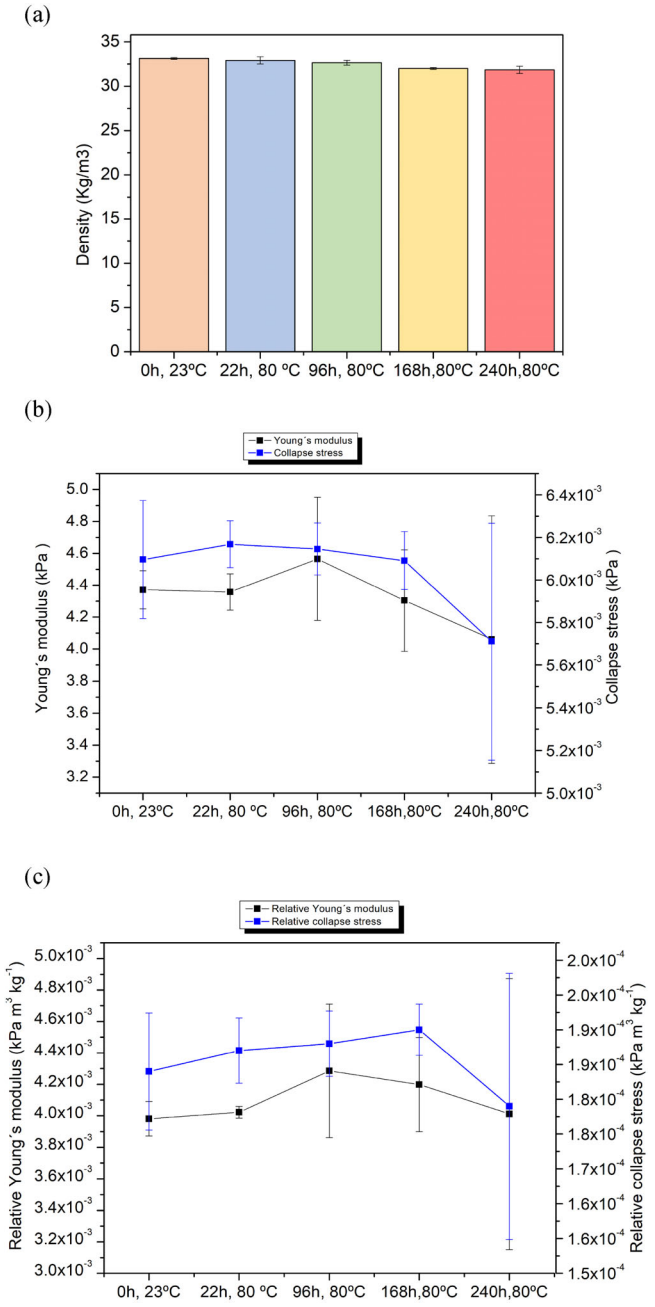

FIGURE 4 (a) Variation of density with time for the sample containing 48.3 pph HFO, (b) Aging of Young's modulus and collapse stress for the sample containing 48.3 pph HFO, (c) Aging of relative Young's modulus and relative collapse stress for the sample containing 48.3 pph HFO. [Color figure can be viewed at wileyonlinelibrary.com]

of these contributions gives the total thermal conductivity (λt)[12,33]:

$$\lambda^t = \lambda^s + \lambda^g + \lambda^r + \lambda^c. \tag{3}$$

The cell size of the foams under study (around 800–900 μm) makes the convective mechanism (λ^c) negligible.[12,33] The conductive terms of the gas and the solid phases can be estimated by Equations 4 and 5[35]:

$$\lambda^g = \lambda g V g, \tag{4}$$

$$\lambda^s = \lambda_s \frac{V_s}{3}\left(\left(f_s\sqrt{\mathrm{AR}}\right) + 2(1-f_s)(\mathrm{AR})^{\frac{1}{4}}\right), \tag{5}$$

where V_g is the volume fraction of the gas phase equal to $(1-\rho_r)$ where ρ_r is the relative density, V_s is the volume fraction of the solid phase equal to ρ_r, AR is the anisotropy ratio, λ_g is the thermal conductivity of gas mixture, λ_s is the thermal conductivity of solid and f_s is the fraction of mass in the struts.

The radiative mechanism refers to the transport of energy by electromagnetic waves, and the attenuation of radiation takes place in the forms of absorption, and scattering. The radiative conductivity can be calculated by the Rosseland equation[12]:

$$\lambda^r = \frac{16n^2\sigma T^3}{3K}, \tag{6}$$

where n is the effective refraction index (close to 1 for low density foams), σ is the Stefan–Boltzmann constant, T is the temperature at which the thermal conductivity is measured, and K is the extinction coefficient of the foam. The radiative conductivity can be estimated with the previous equation (Equation 6) using the approach defined by Glicksman to calculate the extinction coefficient (K_G) as a function of the optical properties of the polymeric matrix and the characteristics of the cellular structure of the foam.

3.4.1 | Extinction coefficient modeling: Glicksman extinction coefficient (K_G)

The Glicksman extinction coefficient (K_G) is calculated here for all systems studied in order to evaluate the radiative contribution. The Glicksman extinction coefficient (K_G) includes the contribution of edges (K_{Edges}) and that of cell walls (K_{Walls})[12]:

$$K_G = K_{\mathrm{Edges}} + K_{\mathrm{Walls}}. \tag{7}$$

$$K_G = \left(4.10\frac{\sqrt{f_s\frac{\rho_f}{\rho_s}}}{\phi}\right) + (1-f_s)\frac{\rho_f}{\rho_s}K_W. \tag{8}$$

This parameter depends on the average cell size (ϕ), foam density (ρ_f), solid matrix density (ρ_s), mass fraction in the struts (f_S), the extinction coefficient of the solid

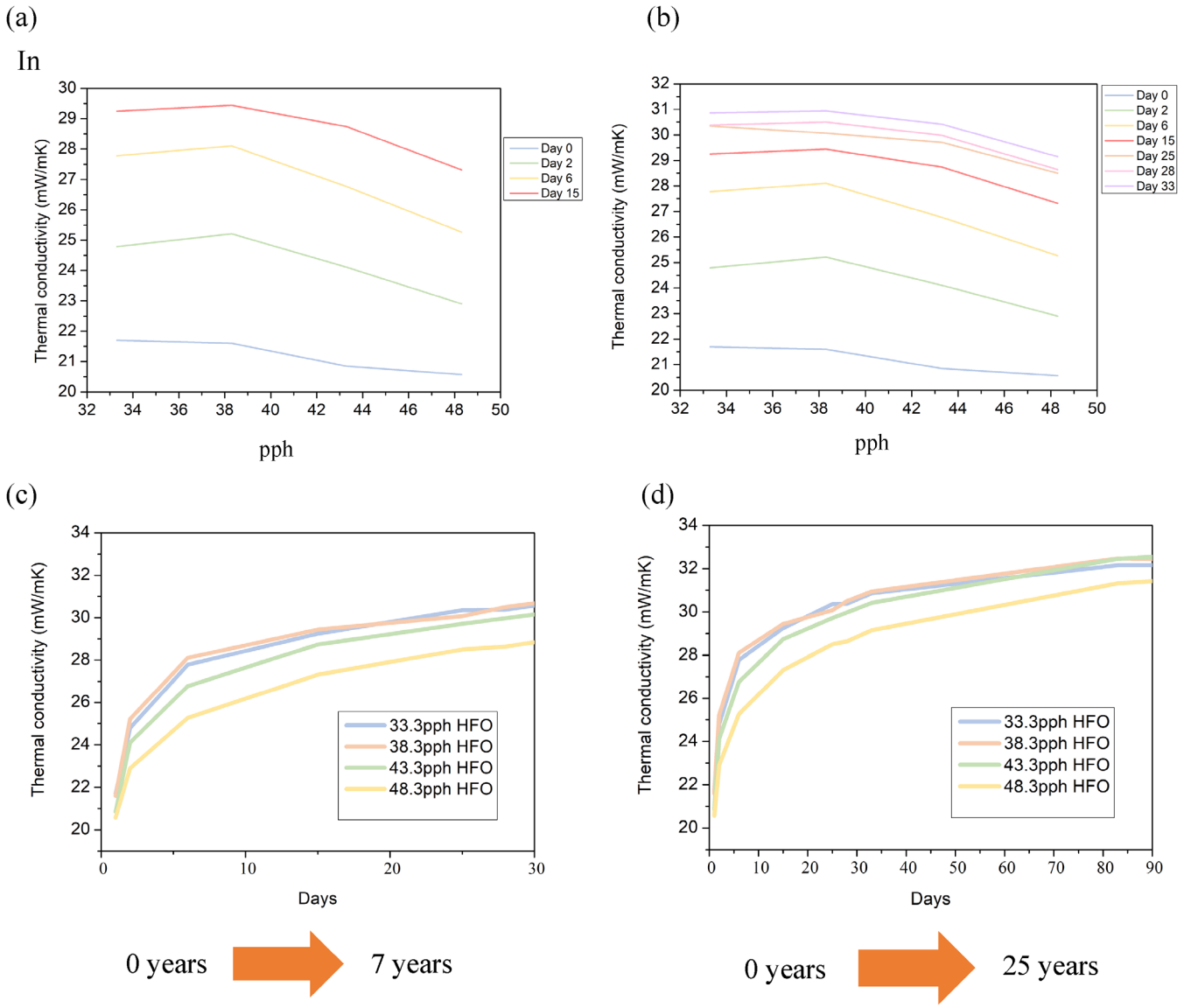

FIGURE 5 Thermal conductivity versus HFO contents between day 0 and day 15 (a) and between day 0 and day 33 (b) and thermal conductivity evolution for different contents of HFO between day 0 and day 30 (c) and between day 0 and day 90 (d). [Color figure can be viewed at wileyonlinelibrary.com]

matrix (K_w) and a constant related to the cell geometry (4.10). The value of f_S was determined by tomography (Table 3), and the value of the extinction coefficient of the solid polymer ($K_w = 600\ cm^{-1}$) was obtained from the literature.[12] The values of the Glicksman extinction coefficients (K_G) calculated using Equation 7 are presented in Figure 9. These data show a decrease of extinction coefficient when the HFO content is increased. The values obtained ranged between 13 and 10 cm^{-1}. This trend of Glicksman extinction coefficient is mainly due to the decrease in foam density when HFO is increased because the cellular structure is very similar for all the analyzed foams, except for sample containing 43.3 pph HFO. This sample presents a minimum in extinction coefficient value which is related to its low density, its higher cell size and the high value of f_s.

This reduction of the extinction coefficient will result in an increment of the radiative contribution for the foams produced with higher amounts of HFO as discussed in the following sections.

3.4.2 | Discussion of the different contributions to the thermal conductivity

Assuming that the conduction through the solid (λ^s) and the radiation (λ^r) are time-independent, the contribution corresponding to the conduction through the gas phase

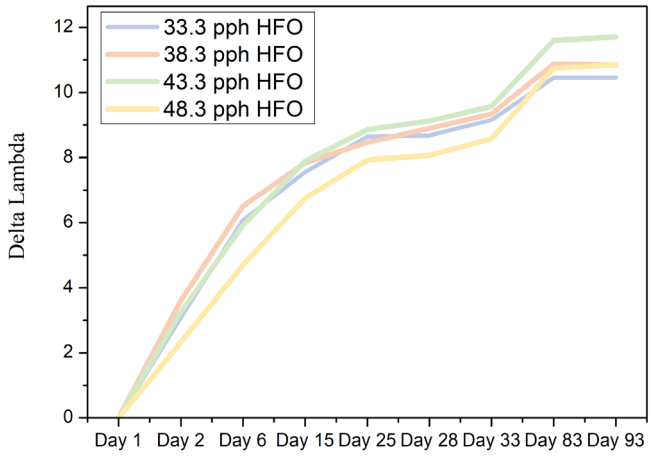

FIGURE 6 Variation of the thermal conductivity measurement during the aging process. [Color figure can be viewed at wileyonlinelibrary.com]

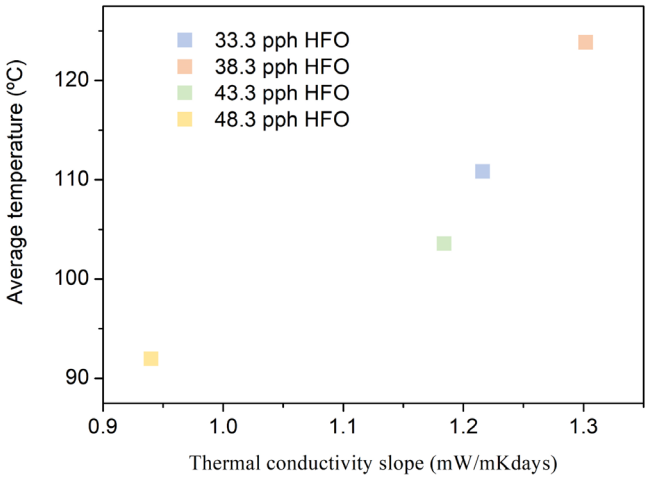

FIGURE 8 Thermal conductivity slope at day 6 as a function of the average temperature reached during foaming. [Color figure can be viewed at wileyonlinelibrary.com]

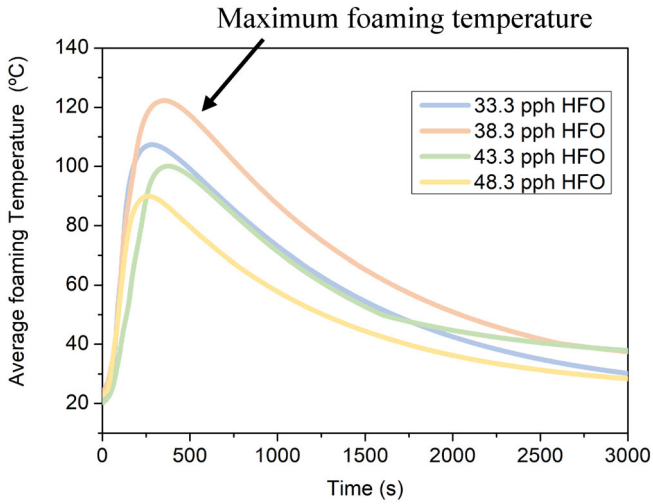

FIGURE 7 Average foaming temperatures as a function of time during the foams production. [Color figure can be viewed at wileyonlinelibrary.com]

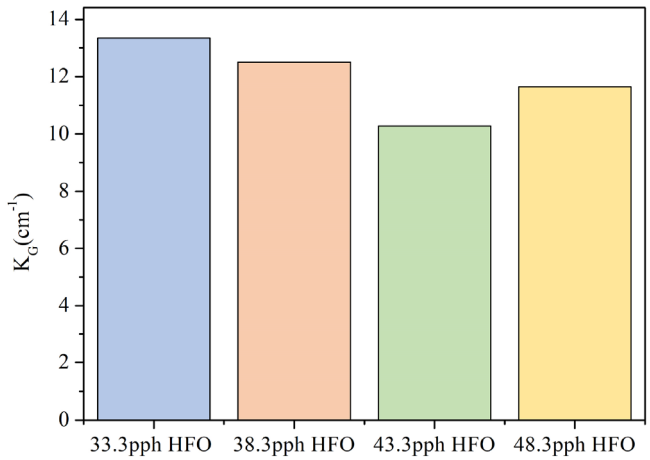

FIGURE 9 Calculated Glicksman's extinction coefficient for the foams under study. [Color figure can be viewed at wileyonlinelibrary.com]

(λ^g) can be calculated using the thermal conductivity model (Equation 3) by subtracting the solid phase contribution (Equation 5) and the radiation contributions (Equations 6 and 8) from the experimental values of the thermal conductivity. The results of this analysis are summarized in the Figures 10–12. As expected, the conduction through the gas phase (λ^g) is the most significant contribution to the final value of the thermal conductivity with a contribution that is in most of the cases higher than 50%. This contribution clearly increases when aging time increases. The value is between 45% and 53% 15 days after production but increases to around 68% to 70% after 90 days of testing. In addition, it is clear that this contribution is smaller for the samples produced with a higher amount of HFO.

The radiation contribution accounts for around 5 mW/m K of the total thermal conductivity, being slightly higher for the samples produced with higher amounts of HFO. In percentage the contribution of this heat transfer mechanisms is between 25% and 32% 15 days after production and around 15%–20% after 90 days.

Finally, conduction through the solid is the mechanism with a lower weight, with a contribution between 3 and 4 mW/m K, being this contribution lower for the samples with a lower density (produced with higher contents of HFO). In percentage this mechanism contributes with a weight of 19% and 21% at 15 days and between 11% and 14% after 90 days.

Taking into account the values of the thermal conductivity for the gas phase it is possible to estimate the

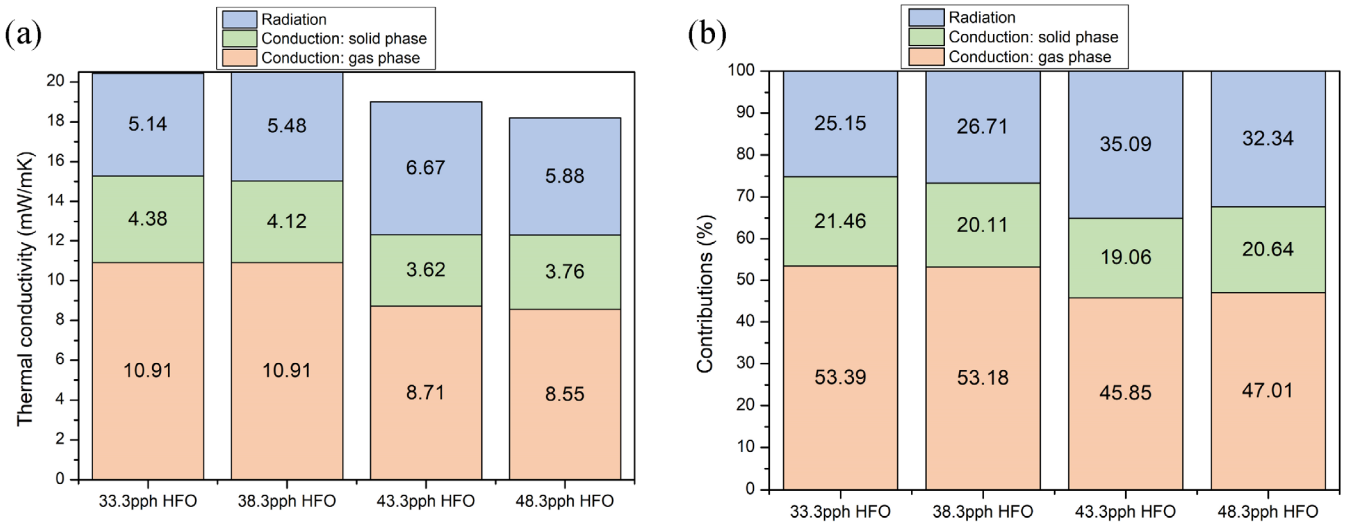

FIGURE 10 (a) The thermal conductivity mechanisms and (b) the contribution of the thermal conductivity mechanisms for each PIR foams at 15 days. [Color figure can be viewed at wileyonlinelibrary.com]

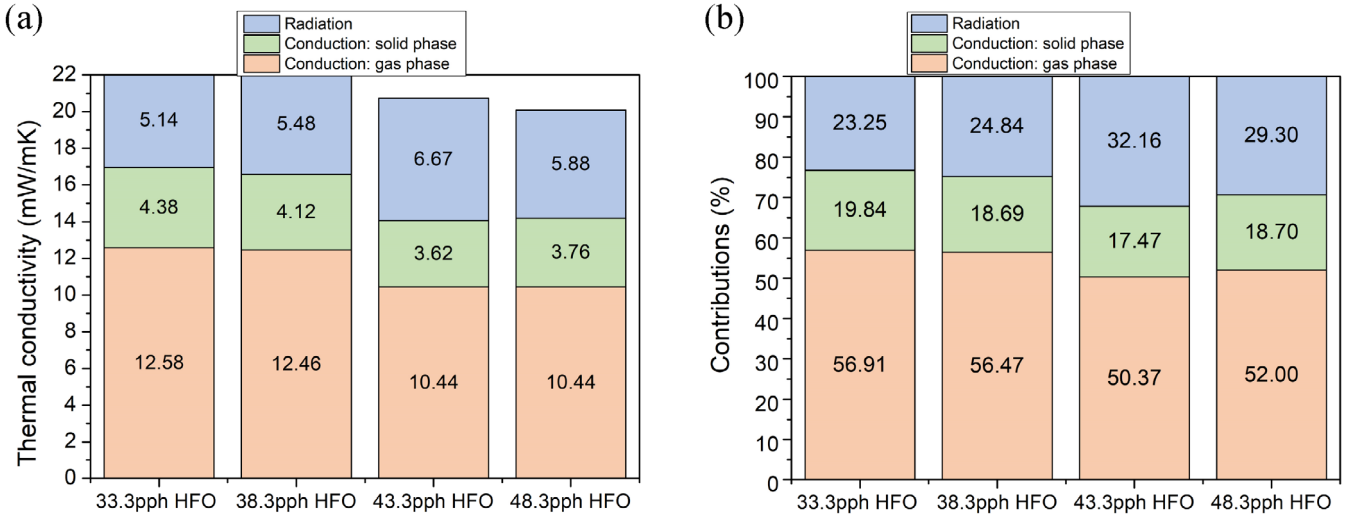

FIGURE 11 (a) The thermal conductivity mechanisms and (b) the contribution of the thermal conductivity mechanisms for each PIR foams at 33 days. [Color figure can be viewed at wileyonlinelibrary.com]

amount of air and HFO in the cells as a function of the aging time. For these calculations we have used the Wassiljeva equation[36]:

$$\lambda_{\text{mix}} = \sum_i \frac{\lambda_i}{1 + \sum_{\substack{j \\ i \neq j}} A_{ij} \frac{x_j}{x_i}}, \tag{9}$$

where λ_m is the thermal conductivity of the mixture, λ_i is the thermal conductivity of pure component i, and x_i and x_j are the mole fractions of components i and j and A_{ij} is a function of the binary system that is typically equal to 1. Figure 13 shows the evolution of gases over time, in the first days it is observed that the amount of air is less than the amount of HFO. With time the amount of air in the cells increases due to the entrance of this gas due to a diffusion mechanisms. By the end of the aging time, 90 days after production, which is equivalent to 25 years of aging, the cells have a composition based on 80% air and 20% of the HFO. The proportion of HFO in the cells is larger for the material produced with a higher amount of HFO, which is the main reason for the lower thermal conductivity of this foam.

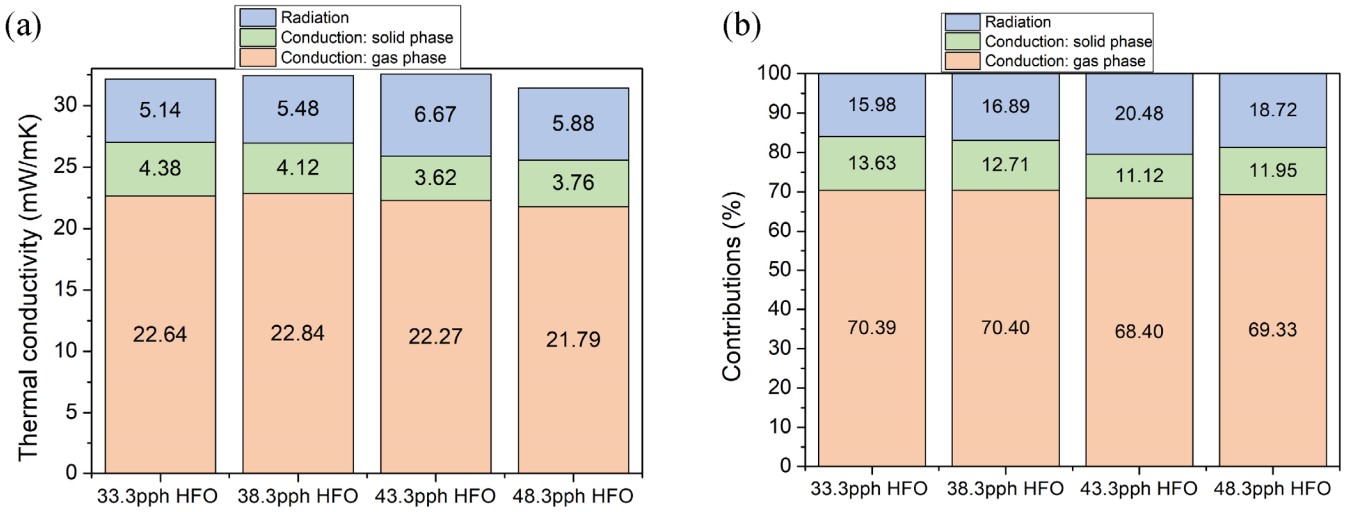

FIGURE 12 (a) The thermal conductivity mechanisms and (b) the contribution of the thermal conductivity mechanisms for each PIR foams at 90 days. [Color figure can be viewed at wileyonlinelibrary.com]

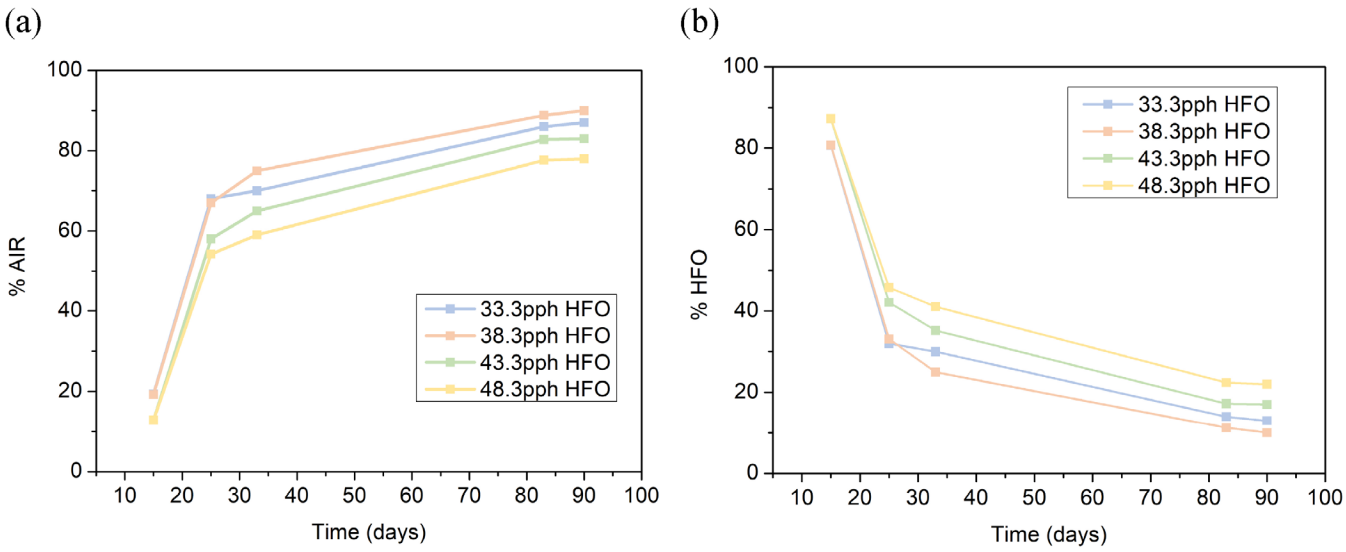

FIGURE 13 Amount of air (a) and HFO (b) in the sample aged for different days. [Color figure can be viewed at wileyonlinelibrary.com]

4 | CONCLUSIONS

In this work, the effect of the content of HFO-1233zd (E) on the temperature during foam production, density, cellular structure, mechanical properties and thermal conductivity of polyisocyanurate (PIR) foams has been evaluated.

As expected, increasing the content of HFO reduced the foams density. Regarding the cellular structure, all materials have similar cellular structures with cell sizes between 800 and 900 microns. Furthermore, these foams have a very homogeneous cellular structure, with a very low open cell content and a slight anisotropy in the growing direction. The fraction of mass in the struts and the cell walls thickness does not follow a clear trend as a function of the HFO content used during production.

As expected, the mechanical properties depend on density with a reduction of the stiffness and strength when density is reduced. However, when the relative properties are analyzed the values obtained are almost constant. In addition, it has been observed that the mechanical properties do not evolve with the aging time.

On the other hand, thermal conductivity aging has been studied using an accelerated laboratory test method that allows predicting thermal conductivity up to 25 years. The initial thermal conductivity of the foams produced is

very low, in the range of 20 to 22 mW/m K. These values increase to reach values in the range of 30 to 32 mW/m K after the aging process. The results have shown that increasing the amount of HFO reduces the thermal conductivity and also the rate of aging in the early stages of aging. The low aging rate has been correlated with a lower temperature during foaming for foams produced with higher amount of HFO. Thus, foams reaching higher foaming temperatures generate a high pressure difference between the inside and the outside of the foam cells once the material is cooled and consequently a very quick diffusion of the gases out of the cells is taking place. Modeling the thermal conductivity of the foams allows quantifying the evolution of the thermal conductivity of the gas mixture (λ_g) with time and estimate the gases content during the aging. It has been demonstrated that even after 90 days of testing, equivalent to 25 years of aging, there is a significant amount of HFO in the gas composition. It has been estimated that 20 of the gas in the cells is HFO.

AUTHOR CONTRIBUTIONS

Patricia Torres-Regalado: Conceptualization (equal); data curation (equal); investigation (equal); writing – original draft (equal). **Mercedes Santiago-Calvo:** Conceptualization (equal). **Josep Gimeno:** Conceptualization and writing – review. **Miguel Angel Rodríguez-Pérez:** Conceptualization, results discussion, writing – review and editing (lead).

ACKNOWLEDGMENTS

Financial support from DI grant DIN2019-010840 (Patricia Torres) from the Spanish Ministry of Economy, Industry, and Competitiveness is gratefully acknowledged. Financial assistance from Ministerio de Ciencia, Innovación y Universidades (MCIU) (Spain) (RTI2018 – 098749-B-I00, PID2021-127108OB-I00, TED2021-130965B-I00, and PDC2022-133391-I00), Regional Government of Castilla y León and the EU-FEDER program (VA202P20), are gratefully acknowledged. This work was supported by the Regional Government of Castilla y León (Junta de Castilla y León), and by the Ministry of Science and Innovation MICIN and the European Union NextGenerationEU/PRTR (C17. I1). We would like to thank Honeywell for supplying the physical blowing agent used in this research.

CONFLICT OF INTEREST STATEMENT

We declare that we have no commercial or associative interest that represents a conflict of interest in relation to the work presented.

DATA AVAILABILITY STATEMENT

The data that support the findings of this study are available from the corresponding author upon reasonable request.

ORCID

Patricia Torres-Regalado https://orcid.org/0000-0001-8057-866X
Mercedes Santiago-Calvo https://orcid.org/0000-0001-7678-5746
Miguel Angel Rodríguez-Pérez https://orcid.org/0000-0002-3607-690X

REFERENCES

[1] R. Heath. *Brydson's Plastics Materials*, Elsevier, Oxford **2017**.
[2] E. Sharmin, F. Zafar, *Polyurethane: An Introduction*, IntechOpen, London **2012**.
[3] M. Kurańska, A. Prociak, S. Michałowski, K. Zawadzińska, *Polimery* **2018**, *63*, 672.
[4] M. Jelena, B. Umberto, *IOP Conf. Ser. Mater. Sci. Eng.* **2019**, *609*, 062016.
[5] M. O. McLinden, M. L. Huber, *J. Chem. Eng. Data* **2020**, *65*, 4176.
[6] M. O. McLinden, J. S. Brown, R. Brignoli, A. F. Kazakov, P. A. Domanski, *Nat. Commun.* **2017**, *8*, 1.
[7] R. S. Grossman, *SAE Int. J. Mater. Manuf.* **2016**, *9*, 794.
[8] A. Galakhova, M. Santiago-Calvo, J. Tirado-Mediavilla, F. Villafañe, M. Á. Rodríguez-Pérez, G. Riess, *Polymers (Basel)* **2019**, *11*, 1192.
[9] S. W. Choi, J. M. Jung, H. M. Yoo, S. H. Kim, W. Il Lee, *Therm. Anal. Calorim.* **2018**, *132*, 1253.
[10] H. Zhang, W. Z. Fang, Y. M. Li, W. Q. Tao, *Appl. Therm. Eng.* **2017**, *115*, 528.
[11] N. V. Gama, A. Ferreira, A. Barros-Timmons, *Materials (Basel)* **2018**, *11*, 1841.
[12] L. R. Glicksman, *Low Density Cellular Plastics: Physical Basis of Behaviour*, Springer, Dordrecht **1994**.
[13] R. Hasanzadeh, T. Azdast, A. Doniavi, M. Rostami, *Heat Mass Transfer* **2019**, *55*, 2845.
[14] A. G. Ostrogorsky, L. R. Glicksman, D. W. Reitz, *Heat Mass Transfer* **1986**, *29*, 1169.
[15] S. Estravís, J. Tirado-Mediavilla, M. Santiago-Calvo, J. L. Ruiz-Herrero, F. Villafañe, M. Á. Rodríguez-Pérez, *Eur. Polym. J.* **2016**, *80*, 1.
[16] Z. Pásztory, T. Horváth, S. V. Glass, S. Zelinka, *Energy Build.* **2018**, *174*, 26.
[17] T. Makaveckas, R. Bliūdžius, A. Burlingis, *J. Build. Eng.* **2021**, *41*, 102447.
[18] A. Tcharkhtchi, S. Farzaneh, S. Abdallah-Elhirtsi, B. Esmaeillou, F. Nony, A. Baron, *Int. J. Polym. Anal. Charact.* **2014**, *19*, 571.
[19] Kairav Chemofarme Industries, Ecofriendly blowing agents for PU foams.
[20] B. Tchanche, G. Papadakis, G. Lambrinos, A. Frangoudakis, *Appl. Therm. Eng.* **2009**, *29*, 2476.
[21] O. Hodnebrog, M. Etminan, J. S. Fuglestvedt, G. Marston, G. Myhre, C. J. Nielsen, W. K. P. Shine, T. J. Wallington, *Rev. Geophys.* **2013**, *51*, 300.
[22] M. Santiago-Calvo, V. Blasco, C. Ruiz, R. París, F. Villafañe, M. Á. Rodríguez-Pérez, *Eur. Polym. J.* **2017**, *97*, 230.
[23] ASTM D1622-08, Standard Test Method for Apparent Density of Rigid Cellular Plastics. **2008**.
[24] ASTM D6226-10, Standard Test Method for Open Cell Content of Rigid Cellular Plastics. **2010**.

[25] M. Santiago-Calvo, J. Tirado-Mediavilla, J. L. Ruiz-Herrero, F. Villafañe, M. Á. Rodríguez-Pérez, *Polym. Int.* **2019**, *68*, 1826.
[26] J. Pinto, E. Solórzano, M. A. Rodriguez-Perez, J. A. De Saja, *J. Cell. Plast.* **2013**, *49*, 555.
[27] S. Pérez-Tamarit, E. Solórzano, A. Hilger, I. Manke, M. A. Rodríguez-Pérez, *Eur. Polym. J.* **2018**, *109*, 169.
[28] C. Petit, S. Meille, É. Maire, *J. Mater. Res.* **2013**, *28*, 2191.
[29] O. Almanza, M. Rodríguez-Pérez, J. de Saja, *Polymer (Guildf)* **2001**, *42*, 7117.
[30] UNE-EN ISO 844:2014, Materiales plásticos celulares rígidos. Determinación de las caracteristicas de compression. **2015**.
[31] UNE-EN ISO 2440:2019, Materiales poliméricos celulares flexibles y rígidos Ensayos de envejecimiento acelerado. **2019**.
[32] British Standards Institution, BS ISO 11561:1999 Ageing of thermal insulation materials — Determination of the long-term change in thermal resistance of closed-cell plastics (accelerated laboratory test methods), pp. 1–24. **1999**.
[33] L. J. Gibson, M. F. Ashby, *Cellular Solids: Structure and Properties*, Pergamon, Oxford **1988**.
[34] M. Santiago-Calvo, J. Tirado-Mediavilla, J. C. Rauhe, L. R. Jensen, J. L. Ruiz-Herrero, F. Villafañe, M. Á. Rodríguez-Pérez, *Eur. Polym. J.* **2018**, *108*, 98.
[35] L. R. Glicksman, *Cell. Polym.* **1991**, *10*, 276.
[36] R. C. Read, J. M. Prausnitz, and T. K. Sherwood, *The Properties of Gases and Liquids*, McGraw-Hill Inc, New York **2000**.

How to cite this article: P. Torres-Regalado, M. Santiago-Calvo, J. Gimeno, M. A. Rodríguez-Pérez, *J. Appl. Polym. Sci.* **2023**, e54504. https://doi.org/10.1002/app.54504